(11) Flory, P. J. *J. Am. Chem. Soc.* **1943**, *65*, 372.
(12) Fox, T. G., Jr.; Fox, J. C.; Flory, P. J. *J. Am. Chem. Soc.* **1951**, *73*, 1901.
(13) Bohdanecky, M.; Kovar, J. *Viscosity of Polymer Solutions*; Elsevier Publishing: New York, 1982.
(14) Ham, G. E. *High Polymers*; Interscience: New York, 1964.
(15) Huggins, M. L. *J. Am. Chem. Soc.* **1942**, *64*, 2716.
(16) Schott, N.; Will, B.; Wolf, B. A. *Makromol. Chem.* **1988**, *189*, 2067.
(17) Schmidt, J. R.; Wolf, B. A. *Macromolecules* **1982**, *15*, 1192.
(18) Herold, F. K.; Wolf, B. A. *Mater. Chem. Phys.* **1986**, *14*, 311.
(19) Flory, P. J. *Principles of Polymer Chemistry*; Cornell University Press: Ithaca, NY, 1953.
(20) De Gennes, P.-G. *Scaling Concepts in Polymer Physics*; Cornell University Press: Ithaca, NY, 1979.
(21) Einstein, A. *Ann. Phys.* **1906**, *19*, 289; *34*, 591.
(22) Holly, E. D. *J. Polym. Sci., Part A* **1964**, *2*, 5267.
(23) Kapuscinski, M. M.; Sen, A.; Rubin, I. D. Presented at the 1989 SAE Fuels & Lubricants Meeting, Baltimore, Sept 1989, SAE Paper No. 892,152.
(24) De Candia, F.; Russo, R.; Vittoria, V. *J. Macromol. Sci.* **1980**, *B18*, 257.
(25) Rietveld, B. J.; Scholte, Th. G. *Macromolecules* **1973**, *6*, 468.
(26) Price, C.; Stubbersfield, R. B. *Eur. Polym. J.* **1987**, *23*, 177.
(27) Higgins, J. S.; Blake, S.; Tomlins, P. E.; Ross-Murphy, S. B.; Staples, E.; Penfold, J.; Dawkins, J. V. *Polymer* **1988**, *29*, 1968.
(28) Price, C.; Hudd, A. L.; Stubbersfield, R. B.; Wright, B. *Polymer* **1980**, *21*, 9.

Rheooptical Study of Isotropic Solutions of Stiff Polymers

D. W. Mead† and R. G. Larson*

AT&T Bell Laboratories, Murray Hill, New Jersey 07974. *Received July 10, 1989; Revised Manuscript Received November 8, 1989*

ABSTRACT: Stresses and birefringences are measured for isotropic solutions of poly(γ-benzyl L-glutamate) as functions of shear rate and time at concentrations ranging from dilute to concentrated. The Doi theory and other Landau-de Gennes theories for rigid molecules predict a pretransitional rise in the stress-optical ratio C—that is, the ratio of birefringence to stress—as the concentration approaches the value at which a first-order liquid-crystalline transition occurs. This predicted rise occurs because of critical slowing down as the concentration approaches the spinodal before being cutoff by the first-order transition. Our measurements of C for PBLG show a rise of this kind by a factor of 3.5. Kinetic rod-jamming effects in our data can be distinguished from the thermodynamic critical slowing down by combined use of stress and birefringence. The Doi theory also predicts a nonlinear coupling between the shearing field and the excluded-volume potential that causes curves of steady-state shear viscosity versus shear rate at different concentrations to cross, an effect seen in our measurements. We find violations of the stress-optical rule in that the measured values of C depend not only on molecular weight and concentration but also on shear rate and time after start-up and cessation of shearing. These latter dependencies can be explained by modest levels of polydispersity in molecular weight.

I. Introduction

The thermodynamics, molecular dynamics, and rheology of straight rigid polymers in solution are strongly dependent on concentration and molecular weight. If the aspect ratio of the rodlike molecules is high (100 or more) and the distribution of molecular weights is not too broad, four regimes of concentration can be discerned, as discussed by Doi and Edwards;[1] see Figure 1. In the dilute and semidilute regimes, the average distance between neighboring rods is so large compared to the rod diameter that they can be regarded as line particles. The semidilute regime is distinguished from the dilute in that in the former molecules are unable to rotate freely without interference from surrounding rods, and in the latter they can. Scaling arguments show that rotational interference becomes significant when

$$\nu L^3 \approx \beta \tag{1}$$

where ν is the number of molecules per unit volume of solution, L is the molecular length, and β is a dimensionless constant that experiments show to be roughly 30.[1]

When the concentration becomes high enough that

$$\nu b L^2 \approx 1 \tag{2}$$

then the rod diameter b is large enough compared to the distance between neighboring rods that excluded volume can no longer be neglected, and the solution is considered concentrated.[1] When excluded-volume effects are modest, the solution remains isotropic at equilibrium, though orientational correlations are present because of packing constraints. At higher concentrations, orientation-dependent excluded-volume effects become so strong that the rods spontaneously orient into a nematic liquid-crystalline phase.

In what follows, we briefly survey the status of theory for the rheology of dilute and semidilute solutions of rigid-rod polymers. We then detail some predictions of the Doi theory for concentrated isotropic solutions of these polymers. Attempts to apply this theory to the liquid-crystalline regime have been hindered by the orientational inhomogeneities (or defects) present in real liquid-crystalline samples and unaccounted for in the theory. The potential of the Doi theory to describe concentrated isotropic solutions, which have no defects, has not heretofore been assessed and is one motivation for the present work.

† Current address: Department of Chemistry & Nuclear Engineering, University of California, Santa Barbara, CA 93106.

0024-9297/90/2223-2524$02.50/0

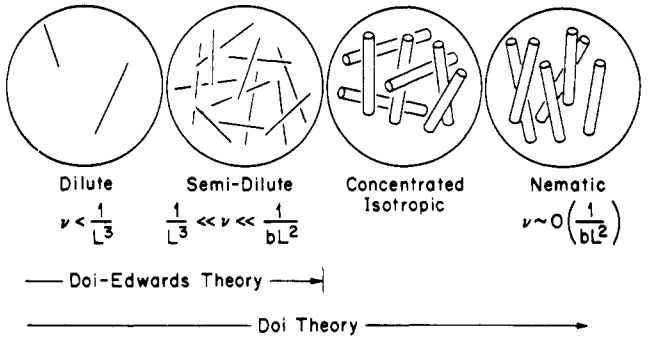

Figure 1. Concentration regimes for long rigid rods in solution according to Doi and Edwards.[1]

II. Theory

The molecular dynamics and rheology of truly rigid molecules are described by a Smoluchowski equation[1]

$$\frac{\partial \psi}{\partial t} + \frac{\partial}{\partial \mathbf{u}}[(\mathbf{u}\cdot\nabla\mathbf{v} - \mathbf{uuu}:\tilde{\mathbf{D}})\psi] - \bar{D}_r \frac{\partial}{\partial \mathbf{u}}\left[\frac{\partial \psi}{\partial \mathbf{u}} + \psi \frac{\partial}{\partial \mathbf{u}}\left(\frac{U_{scf}}{kT}\right)\right] = 0 \quad (3)$$

where $\psi(\mathbf{u})$ is the probability that a rod has an orientation given by the unit vector $\mathbf{u}$. $\nabla\mathbf{v}$ is the velocity gradient, $\tilde{\mathbf{D}} \equiv {}^1/_2(\nabla\mathbf{v} + \nabla\mathbf{v}^T)$ is the rate of deformation tensor, $\bar{D}_r$ is an effective rotary diffusivity, and U_{scf} is an effective excluded-volume potential. In the dilute and semidilute regimes, U_{scf} can be neglected. Dilute solutions are distinguished from semidilute solutions by the behavior of the effective rotary diffusivity.

A. Dilute Regime. In the dilute regime, the rotary diffusivity is a simple constant

$$\bar{D}_r = D_{r0} \quad (4)$$

that scales as $\ln(M)/M^3$, where M is the molecular weight.[1] The stress tensor σ is given by

$$\tilde{\sigma} = \underbrace{\frac{\nu\zeta L^2}{2}\langle \mathbf{uuuu}\rangle:\tilde{\mathbf{D}}}_{\text{viscous}} + \underbrace{3\nu kT\left[\langle \mathbf{uu}\rangle - \frac{1}{3}\tilde{\delta}\right]}_{\text{viscoelastic}} \quad (5)$$

where the brackets denote an average over the orientation distribution function ψ, for example

$$\langle \mathbf{uu}\rangle \equiv \int \mathbf{uu}\psi \, du^2 \quad (6)$$

For future reference we also define an order parameter tensor $\tilde{\mathbf{S}}$:

$$\tilde{\mathbf{S}} \equiv \left[\langle \mathbf{uu}\rangle - \frac{1}{3}\tilde{\delta}\right] \quad (7)$$

The first term in eq 5 arises from drag the solvent exerts as it flows around the rods; ζ is a friction coefficient that is proportional to the solvent viscosity. With these equations, rheological properties of dilute solutions of rigid polymers such as tobacco mosaic virus have been calculated and are found to agree well with experiments.[2]

B. Semidilute Regime. In the semidilute regime, Doi and Edwards have obtained $\bar{D}_r$ from a model wherein each rod is supposed to reside in a cage created by the neighboring rods.[1] The cage limits a rod's rotational freedom to a small angle ϵ where $\epsilon \sim a/L$ and a is the cage size and L the rod length. From scaling arguments, a is proportional to $1/\nu L^2$. The rod can completely reorient only by a compound process in which it repeatedly escapes from its cage by translational diffusion, each time rotating by a small random angle of roughly ϵ. The effective rotary diffusivity produced by this compound process is

$$D_r = \epsilon^2/\tau_D \approx \left(\frac{a}{L}\right)^2 D_{r0} = \left(\frac{1}{\nu L^3}\right)^2 D_{r0} \quad (8)$$

Here τ_D is the time required for the rod to diffuse a rod length L along its own axis; this time is found to be approximately $1/D_{r0}$. If the rod concentration is expressed in terms of volume fraction $\phi \propto \nu/L$, then considering the scaling of D_{r0} with molecular weight M, one finds that

$$D_r \propto \phi^{-2} M^{-7} \ln(M) \quad (9)$$

If the rods have a net average orientation because of flow or body forces, Doi and Edwards argued that the cage diameter a is dilated according to

$$\bar{D}_r \equiv D_r\left[\frac{4}{\pi}\int\int \psi(\mathbf{u})\,\psi(\mathbf{u}')|\mathbf{u}\times\mathbf{u}'|\,du^2\,du'^2\right]^{-2} \quad (10)$$

With the Smoluchowski equation (3) and eqs 8 and 10, one can calculate stresses in a semidilute solution of rods using eq 5 for the stress tensor. Because the rotary diffusivity becomes so small when M is large, strain rates that are too small to produce a significant viscous contribution to the stress tensor can still substantially orient the molecules and produce large viscoelastic contributions.[1] Under these conditions, the viscous contribution in (5) can be dropped leaving

$$\tilde{\sigma} = 3\nu kT\tilde{\mathbf{S}} \quad (11)$$

Since the birefringence is also proportional to $\tilde{\mathbf{S}}$, one expects the *stress–optical law* to hold

$$\tilde{\mathbf{n}} = C\tilde{\sigma} \quad (12)$$

where $\tilde{\mathbf{n}}$ is the anisotropy in the index of refraction tensor (i.e., the birefringence) and C is the stress–optical coefficient. The stress–optical law has usually been found to hold for melts and solutions of flexible polymers.[3] In these systems, the stress–optical coefficient is independent of molecular weight, nearly independent of concentration, and independent of strain rate as long as the flexible molecules are not stretched to nearly full extension.[3,4] For rodlike polymers, one expects C to be much larger than for flexibles and to depend on molecular weight. Because the anisotropy in polarizability of a long rodlike molecule is proportional to its length—that is, there is a constant anisotropy in polarizability per unit molecular length—for a given level of orientation the birefringence depends only on the mass fraction of polymer and not on the molecular length. The viscoelastic stress, however, is produced when configurational entropy is reduced from its equilibrium level as a result of flow-induced orientation. Thus the more orientation (and hence birefringence) one obtains per unit of entropy reduction, the higher the stress–optical coefficient. Long rods have fewer degrees of freedom per unit volume of material than do flexible chains, and hence less entropy must be extracted from a system of rigid molecules than from flexible molecules to attain the same degree of alignment. If the rod is stiff, the number of degrees of freedom per unit length of rod is inversely proportional to the rod length; hence the stress–optical coefficient for solutions of rigid rods is expected to be high compared to that for flexibles and to increase linearly with molecular weight. Thus, for example, if one chops long rods in half, the amount of entroy that one must extract from the chopped rods to align them is double that amount one must extract from the original rods to obtain the same alignment. Hence C for the chopped rods is half that of the original rods. Tsvetkov and co-workers[5] have measured stress–optical coefficients as functions of molecular weight M for a variety of stiff and not-so-stiff polymers in the dilute-solution regime. This

body of work shows that in general C increases linearly with M until the molecular length exceeds roughly one persistence length; at higher molecular weights C approaches a plateau and becomes independent of M when M is high enough that the molecule can be considered flexible. For poly(γ-benzyl L-glutamate) in dichloroethane, significant deviations from linearity between C and M occur when $M \approx 100\,000$–$200\,000$. A plateau in C in excess of 1.3×10^{-7} cm^2/dyn is approached as M exceeds 400 000. This value of C is about 3 orders of magnitude larger than the value typically found for flexible polymers.[3] Because rods of different molecular weight have different stress–optical coefficients, and rods of different length in the semidilute regime relax their orientational order at very different rates according to eq 8, one should not expect the stress–optical law to hold in any of the concentration regimes if the rods are polydisperse. This expectation does not yet seem to have been tested experimentally and is addressed in what follows.

By solving eq 3 numerically (with $U_{scf} = 0$ in the semidilute regime), one can obtain "exact" results for the stress $\tilde{\sigma}$ and the birefringence $\tilde{\mathbf{n}}$ from eqs 11 and 12. Alternatively with the aid of decoupling approximations, an equation for the time evolution of the order parameter tensor $\tilde{\mathbf{S}}$ can be derived from eq 3. From this equation one can solve approximately for $\tilde{\mathbf{S}}$, and thereby $\tilde{\sigma}$ through eq 11, without having first to solve for the distribution function ψ. Chow et al. have carried out both the exact and the decoupling procedures to predict the shear-rate and time-dependent birefringence of semidilute solutions of collagen, which is a reasonably rigid molecule.[6] In particular, they have shown that plots of birefringence versus shear rate scale with collagen concentration as predicted by the semidilute theory of Doi and Edwards. Using the exact treatment, quantitative agreement between the theory and experiment for the shear-rate dependence of the birefringence was obtained after accounting for the effects of polydispersity in molecular weight. Though their samples were described by low levels of polydispersity—having ratios of weight-to-number average molecular weights (M_w/M_n) of around 1.1—rotary diffusivities are so sensitive to molecular weight in this concentration regime that one must account for the effects of polydispersity, if quantitative agreement with theory is sought.

C. Concentrated Isotropic Regime. For polymer concentrations above those of semidilute solution, additional complications enter; so far even qualitative agreement between experiment and theory in the concentrated isotropic regime has not been shown, except perhaps for zero-shear viscosities. The concentrated isotropic regime is simpler than the nematic regime since the solution remains isotropic at equilibrium but is more complex than the semidilute regime since the self-consistent excluded-volume potential U_{scf} cannot be ignored. In the presence of flow, this potential assists the imposed mechanical forces in inducing orientation and thus enters into the relationship between orientation and stress. The simplest useful form to take for the excluded volume potential is that of Maier and Saupe[1]

$$U_{scf} = \text{const} - {}^3/_2 UkT\mathbf{uu}:\langle\mathbf{uu}\rangle \tag{13}$$

U is a coefficient that is proportional to concentration. With this form for U_{scf}, the evolution equation for $\tilde{\mathbf{S}}$ can be obtained from eq 3 by using a decoupling approximation[1]

$$\frac{\partial}{\partial t}\tilde{\mathbf{S}} = \tilde{\mathbf{F}}[\mathbf{S}] + \tilde{\mathbf{G}}[\tilde{\mathbf{S}}] \tag{14}$$

where

$$\tilde{\mathbf{F}} \equiv -6\bar{D}_r\left[\left(1 - \frac{U}{3}\right)\tilde{\mathbf{S}} - U\left(\tilde{\mathbf{S}}\cdot\tilde{\mathbf{S}} - \frac{1}{3}\tilde{\mathbf{S}}:\tilde{\mathbf{S}}\tilde{\delta}\right) + U\tilde{\mathbf{S}}\tilde{\mathbf{S}}:\tilde{\mathbf{S}}\right] \tag{15}$$

$$\tilde{\mathbf{G}} \equiv \frac{2}{3}\tilde{\mathbf{D}} + \nabla\mathbf{v}^T\cdot\tilde{\mathbf{S}} + \tilde{\mathbf{S}}\cdot\nabla\mathbf{v} - \frac{2}{3}\tilde{\mathbf{D}}:\tilde{\mathbf{D}}\tilde{\delta} - 2\tilde{\mathbf{D}}:\tilde{\mathbf{S}}\tilde{\mathbf{S}} \tag{16}$$

Equation 10 for the rotary diffusivity is approximated by

$$\bar{D}_r = D_r\left[1 - \frac{3}{2}\tilde{\mathbf{S}}:\tilde{\mathbf{S}}\right]^{-2} \tag{17}$$

The work done against the excluded-volume potential when a material element is deformed produces a contribution $\tilde{\sigma}_{scf}$ to the stress tensor:

$$\tilde{\sigma} = 3\nu kT\tilde{\mathbf{S}} + \tilde{\sigma}_{scf}$$

$$\tilde{\sigma} = 3\nu kT\tilde{\mathbf{S}}\left(1 - \frac{U}{3}\right) - 3\nu kTU\left[\tilde{\mathbf{S}}\cdot\mathbf{S} + \frac{1}{3}\tilde{\mathbf{S}}:\tilde{\mathbf{S}}\tilde{\delta} + \tilde{\mathbf{S}}:\tilde{\mathbf{S}}\tilde{\mathbf{S}}\right] \tag{18}$$

Note that the sign of the excluded volume term $\tilde{\sigma}_{scf}$ is opposite that of the ordinary semidilute stress. Thus the nematic potential, as expected, reduces the amount of stress required to achieve a given level of orientation.

Equations 14–18 are the standard equations of the Doi theory for concentrated solutions of rodlike polymers.[1] As presented here, the theory strictly applies to solutions of rodlike polymers that are *monodisperse* in length.

In the small-deformation region of linear viscoelasticity, only the first term $3\nu kT\tilde{\mathbf{S}}(1 - U/3)$ is important. From this term, we see that the stress–optical coefficient ought to be affected by concentration:

$$C \propto \frac{1}{1 - U/3} = \begin{cases} 1 & U \to 0 \\ \infty & U \to 3 \end{cases} \tag{19}$$

As U approaches the value 3, the stress–optical coefficient is expected to rise toward a singularity. The singularity is not reached because it occurs at the spinodal concentration; a first-order phase transition to the liquid-crystalline state cuts off this increase. Nevertheless, a significant increase before the transition is expected. This rise reflects the increasing indifference of the isotropic system to orientation as the concentration approaches the point where the system *prefers* a net equilibrium orientation over isotropy. Thus the closer one comes to the concentration at which the system spontaneously orients, the smaller the stress required to produce a given level of orientation, and the higher the value of C. Pretransitional effects should be expected whenever an orienting field is applied at concentrations close to the liquid-crystalline transition.[7] Nakamura and Okano[8] have already reported pretransitional effects obtained when semirigid bacterial viruses were oriented by a magnetic field. To our knowledge, a pretransitional rise in C has not heretofore been reported.

In general C will rise by the factor $(1 - \nu_1/\nu^*)^{-1}$ as the concentration ν is increased from $\nu \ll \nu^*$ to ν_1, where ν_1 is the concentration at which the first-order transition occurs and ν^* is the spinodal concentration where the isotropic phase becomes unstable to small orientational perturbations. From Onsager's original calculation[9] for solutions of rods one obtains a pretransitional rise, $(1 - \nu_1/\nu^*)^{-1}$ of 6, while from a later more refined calculation[10] one obtains a value of 5.64. Since one expects dispersity in molecular weight to broaden the first-order transition,[11] most experimental systems will probably show pretransitional rises in C that are less than the theoretical values for monodisperse perfectly rigid rods.

Table I
Concentration Scaling in the Concentrated Isotropic Regime

linear viscoelastic property	scaling with concn
stress–optical coefficient, C	$(1 - U/3)^{-1}$
relaxation time, λ	$\nu^2(1 - U/3)^{-1}(1 - B\nu/\nu_1)^{-2}$
high-frequency modulus, G	$\nu(1 - U/3)$
zero-shear viscosity, η_0	$\nu^3(1 - B\nu/\nu_1)^{-2}$

Another pretransitional phenomenon is the predicted increase in the rotational relaxation time λ with concentration:

$$\lambda = \frac{1}{6\bar{D}_r(1 - U/3)} \tag{20}$$

Thus λ increases by a factor of $(1 - U/3)^{-1}$ more steeply than is predicted by semidilute scaling for $\bar{D}_r$ because of the nearness of the spinodal concentration. The effect occurs because the near indifference of the system to an imposed orientational perturbation makes that perturbation slow to relax. We may thus refer to this effect as critical slowing down.

In addition to this thermodynamic pretransitional effect, Doi[12] has considered a kinetic effect that is referred to as *rod jamming* and is produced by excluded volume. Scaling arguments show that the transition to a liquid-crystalline state occurs at a concentration at which the rod diameter b is only slightly smaller than the cage diameter a. If b were to equal a, the rod would be completely unable to rotate. The kinetic rod-jamming effect can be distinguished conceptually from critical slowing down by a gedanken experiment in which line particles orientationally order because of anisotropic forces (perhaps van der Waals) that are not of excluded-volume origin. This imaginary system would show critical slowing down with no rod-jamming effects. Doi proposed that rod jamming be accounted for by multiplying the rotary diffusivity by a simple factor $(1 - B\nu/\nu_1)^2$, where B is a dimensionless constant that is slightly less than unity. Edwards and Evans[13] have derived a somewhat different form for this factor. Table I shows how various linear viscoelastic properties should scale with concentration in the concentrated isotropic regime. Keep in mind that U is proportional to ν.

Under stronger flow fields, nonlinear effects become important, and the terms quadratic and cubic in $\tilde{\mathbf{S}}$ in eq 18 enter. Under these conditions, the stress–optical ratio n_{12}/σ_{12} is predicted to depend on shear rate, as Figure 2 shows. Here the Deborah number De is defined to be $\dot{\gamma}\lambda$, the shear rate multiplied by the relaxation time. These curves were generated by integrating numerically eq 14 to steady state starting with $\tilde{\mathbf{S}} = 0$—i.e., equilibrium—at $t = 0$. Figure 2 shows that for concentrations close to ν_1, shearing can induce a precipitous and even discontinuous rise in C. The numerical integration shows that steady-state solutions to eq 14 that correspond to liquid-crystalline states can be induced for U slightly less than $^8/_3$ by shearing at a sufficiently high shear rate. $^8/_3$ is the minimum value of U for which a static anisotropic solution of eq 14 exists. The critical shear rate at which the nematic state is induced may not be given precisely by these calculations since they neglect effects of concentration fluctuations. We also do not known the precise value of U at which the first-order transition should occur. $^8/_3$ is the minimum value of U for which a static anisotropic solution of eq 14 exists.

When the liquid crystalline state is induced by shearing, the birefringence is predicted to rise and the stress to fall. Figure 3 shows the predicted viscosity as a function of shear rate and U. The viscosity of solutions with concentration close to the transition can crossover and drop below those of solutions of lesser concentration as the shear rate increases. Thus at increased shear rates the viscosity can depend inversely on concentration, just as it does in the nematic concentration range. Crossover occurs continuously if the concentrations are not too near the transition. At higher concentrations, discontinous crossovers—i.e., shear-induced phase transitions—occur. At the highest shear rates, the effects of the nematic potential are swamped by flow effects, and a second, reverse, crossover occurs and the solutions of highest concentration are again predicted to be the most viscous.

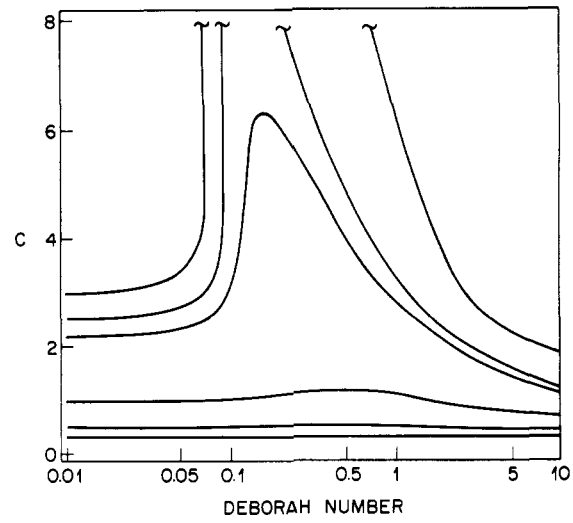

Figure 2. Doi theory predictions for the stress–optical coefficient C as a function of Deborah number = $\dot{\gamma}\lambda$ where $\dot{\gamma}$ is the shear rate and λ is the relaxation time at zero-shear rate. Each curve corresponds to a different value of U. From the lowest curve to the highest the values of U are 0.5, 1.0, 2.0, 2.5, 2.6, and 2.66.

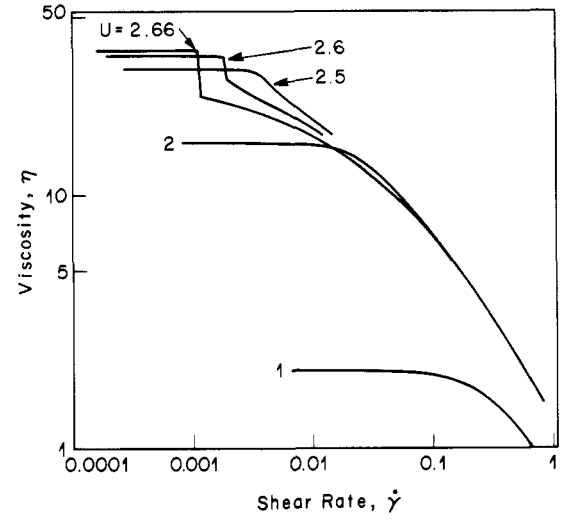

Figure 3. Prediction of the Doi theory for the viscosity as a function of shear rate and the excluded-volume parameter U, which is proportional to concentration ν. In this plot, the units of concentration are chosen so that $U = \nu$; the units of time are such that $6\bar{D}_r = 1$ at $U = 1$ and $\dot{\gamma} \to 0$; stress is in units of kT.

According to eq 18, the stress tensor $\tilde{\sigma}$ is proportional to $\tilde{\mathbf{S}}$ and products of $\tilde{\mathbf{S}}$ that are also coaxial with $\tilde{\mathbf{S}}$. This coaxiality means that various component stress–optical ratios, such as n_{12}/σ_{12} and $(n_{11} - n_{22})/(\sigma_{11} - \sigma_{22})$ etc., must be equal to each other, even though these ratios can depend on concentration or shear rate. The simplest test for this in simple shear is to check for equality

between the optical extinction angle χ_{opt} and its mechanical counterpart:

$$\tan(2\chi_{mech}) \equiv \frac{2\sigma_{12}}{\sigma_{11}-\sigma_{22}} = \frac{2n_{12}}{n_{11}-n_{22}} \equiv \tan(2\chi_{opt}) \quad (21)$$

Thus we draw a distinction between the scalar stress–optical *coefficient* and component stress–optical *ratios*. The stress–optical coefficient is the proportionality constant C of eq 12 *when the stress and birefringence tensors are proportional and coaxial to each other*, i.e., when the stress–optical law holds over some range of shear rate. When the stress–optical law fails, we may still take the ratio of 2 respective components of these tensors, the 12 components for instance, and call this a stress–optical ratio, which can depend on shear rate and on the particular tensor components used to form the ratio.

To sum up this section, three important effects are expected in the concentrated isotropic regime: critical slowing down and rod jamming—which are observable in the linear viscoelastic regime—and a nonlinear coupling between the shear field and the excluded-volume potential that causes a crossing of viscosity–shear rate curves.

III. Experimental Section

A. Materials. PBLG [poly(γ-benzyl L-glutamate)] samples (lot 81994) obtained from Polysciences were dissolved in *m*-cresol. By viewing the material under a polarizing microscope we found that at room temperature the solutions begin to show signs of biphasic character at concentrations around 9.5%. The material is completely liquid crystalline at concentrations of 13% or higher.

The molecular weight of our PBLG sample from Polysciences was estimated to be 230 000. This estimate was obtained from several considerations. First, the concentration dependence of the zero-shear viscosity of our PBLG sample in *m*-cresol is nearly the same as that of a sample of Hermans in the same solvent that he reported had a molecular weight of 270 000.[14] Hermans used an intrinsic viscosity measurement in the nonhelicogenic solvent dichloroacetic acid to obtain this value for the molecular weight. We measured an intrinsic viscosity of our sample in the helicogenic solvent *m*-cresol of 375 cm^3/g, about 35% less than the value Hermans measured for his 270 000 molecular weight sample in *m*-cresol. From our measured intrinsic viscosity and eq 8.138 of Doi and Edwards,[1] which predicts the intrinsic viscosity of solution rigid rods from the molecular weight of the rods, we obtain an estimated molecular weight of about 230 000. From these considerations, we believe that our sample has a viscosity-averaged molecular weight of about 230 000. The results of a GPC study[17] of this and other samples of PBLG (in dimethylformamide with 2.5% dichloroacetic acid added to prevent molecular aggregation) were also consistent with an average molecular weight of roughly 230 000 for the sample discussed here. This value corresponds to a molecular length of 155 nm, yielding a length-to-diameter aspect ratio of about 102. The molecular weight of our material is a convenient one, since shorter molecules relax faster and are therefore harder to probe rheologically, and significantly longer molecules are too long compared to their persistence length (which is around 90 nm in *m*-cresol[15]) to be considered even approximately rigid.[16] From the GPC study, we also obtained an estimated polydispersity index, M_w/M_n, of 1.8. This level of polydispersity is similar to that of other samples of PBLG, including those supplied by Sigma Chemical.[17]

Studies on this sample of PBLG at concentrations in the liquid-crystalline regime were reported earlier.[18] Here we consider only solutions of this material with concentration c of less than or equal to 9.5% by weight. We also consider a second polymer, PBLG from Sigma with a molecular weight of 23 000 as reported by Sigma. Except where otherwise noted, all experiments were done at 29 °C.

B. Rheometry. Five instruments were used, the Rheometrics stress rheometer (RSR-8600) with a Couette fixture described earlier, the Rheometrics fluids rheometer (RFS-8400) with a cone-and-plate fixture (radius = 25 mm, cone angle = 0.02°), the Rheometrics system 4[19] with a steady shear head and a cone-and-plate fixture (radius = 25 mm, cone angle = 0.04°), capillary rheometers (Canon-Ubbelohde sizes 200 and 350), and a rheooptical device for measuring stress and birefringence simultaneously, thereby allowing determination of stress–optical ratios. The stress and fluids rheometers could accommodate maximum torques of 100 g·cm, the system 4 was fitted with a 2000 g·cm transducer, and the transducer for the rheooptical device permitted interchanging of springs, thereby allowing measurement over a wide range of torques, down to 0.1 g·cm or so, a limit imposed by sensitivity to vibrations.

Stress–optical coefficients have in the past been determined by separately performing mechanical and optical experiments and thereafter combining the data. Only one instrument successfully combined both optical and mechanical measurements; however the optics were not capable of simultaneously measuring both the birefringence and extinction angle.[20] Hence, separate experiments were required to determine completely the relevant optical quantities. For time-dependent measurements, this method can be inadequate because small errors in synchronization or random experimental fluctuations seriously reduce the precision with which one can measure stress–optical ratios. Such errors become intolerable when one attempts to detect small violations in the stress–optical rule. Simultaneous measurement of stress and birefringence is especially important for a study of isotropic solutions of rigid rods, where significant deviations in the stress–optical rule are expected; see section II.C.

In optical measurements in shear normally *two* pieces of information are required, namely, birefringence and the extinction angle. However, only *one* optical quantity, the light intensity, can be measured at any instant. Frattini and Fuller,[21] however, have devised an optical apparatus that modulates the retardation at a frequency much higher than the time scale for signifiant change in fluid properties. This provides a carrier wave that is then frequency and amplitude modulated by the time-dependent optical properties of the fluid. The resulting complex waveform is separated into its first and second principal Fourier components, thus providing two measurable quantities that are measured virtually simultaneously at each instant in time; these can be converted into a birefringence and an orientation angle.

The optical instrumentation has been well established by earlier workers.[21,22] Here we extend the capabilities of the instrument by coupling the optical measurements to mechanical measurements. To do this, a torque transducer was designed, constructed, and placed in the instrument. The rigid geometric constraints imposed by the optics preclude the use of any off-the-shelf transducer. Our transducer is capacitive but differs from most of this type in that the capacitance is *not* referenced to ground and in that nonlinearity is deliberately introduced by enhance the sensitivity and resolution. Not referencing the transducer to ground improves the sensitivity from first to second order in small changes in the stray capacitance, thereby producing a cleaner signal than is typically generated from transducers of this type. In our transducer, the torque T is related to the voltage V signal through the following relation

$$T = \frac{C_1}{V} + C_2$$

where C_1 and C_2 are experimentally determined calibration constants. These calibration constants can be varied by adjusting the initial gap between the parallel capacitor plates with a micrometer attached to one of the plates. In this manner, the sensitivity and resolution can be adjusted on an experiment-by-experiment basis. Practically, the transducer could resolve 0.1 g·cm and was limited by stray mechanical vibrations, not the intrinsic design limits.

The flow cell used in the rheooptical work is of Couette type, with an inner diameter of 0.90 in. and an outer diameter of 1.00 in. Two inner cylinders were designed. The long one is 1.375 in. long corresponding to an aspect ratio of gap length to width of more than 25:1, the short one is 0.5 in. long and the gap ratio

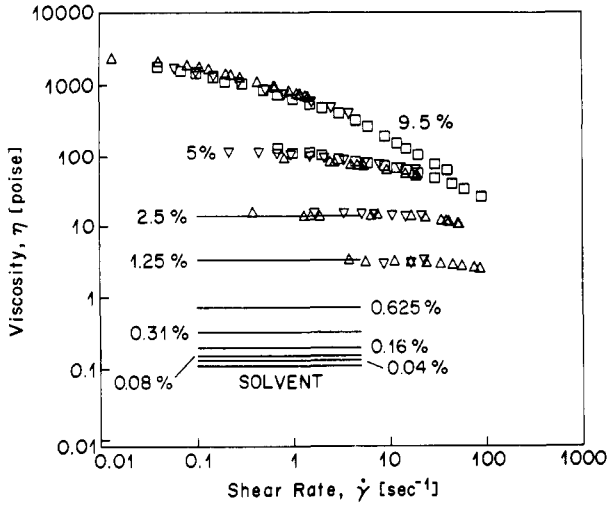

Figure 4. Viscosity of PBLG solution as a function of shear rate as measured on capillary rheometers (lines), the stress rheometer (▽), the fluids rheometer (□), and the rheo-optical device (▽).

10:1. Results obtained for these two cylinders were very similar, and only results from the shorter of the two are reported here. We here neglect end effects and assume the flow to be two-dimensional. A drag flow is generated by rotation of the outer cup while the inner bob remains stationary. A computer-controlled stepper motor drives the system. Torque measurements are made at the stationary inner bob. The bottom of the bob is of conical shape with cone angle selected such that the shear rate at the rotating bottom plate is identical with that in the gap, thereby minimizing end corrections. Because of curvature effects from the finite ratio of gap to bob radius, the shear rate in the Couette cell varies ±10% from the mean value.

The laser beam passes through a small window mounted on top of the Couette cell, through the neutral direction of the shearing field of the fluid and out of the flow cell through the bottom rotating plate. Heating is accomplished by using resistive electrical bands wrapped around a massive aluminum block that contains the cup and bob assembly. Lubricating fluid filling a small gap 0.005 in. thick between the stationary block and the rotating cup conducts the heat to the cup and thence to the polymeric fluid. A thermocouple embedded in the block and an electronic controller permit stable temperature control.

IV. Results

Figure 4 shows shear viscosities obtained on four devices as functions of shear rate and concentration. The agreement among the various instruments is good, except for the 9.5% solution, for which the rheooptical device shows a viscosity about 20% higher than that obtained on three other instruments, including the system 4. The 9.5% solution is extremely close to the liquid-crystalline transition, and its viscosity may be especially sensitive to temperature variations and small amounts of solvent evaporation. The capillary viscometry data were obtained at shear rates low enough that the fluid is Newtonian; the lines in Figure 4 are there to show that these are low shear-rate viscosities and should not be interpreted as representing a range of shear rates over which the measurements were made. To the solvent, metacresol, PBLG was added in concentrations ranging from 0.03906% (w/w) to 9.5%. Each successive concentration in Figure 4 doubles the preceding. Concentrations of 0.156% and less are roughly in the dilute range, as shown by an approximate proportionality between the viscosity increment due to polymer and the concentration. The intrinsic viscosity of the polymer is 375 cm^3/g. At concentrations (c) of 0.3125% and above, large relative increases in viscosity occur with each doubling of concentration, indicating that the solutions are entering the semidilute range where viscosity should scale as c^3 and the relaxation time as c^2.

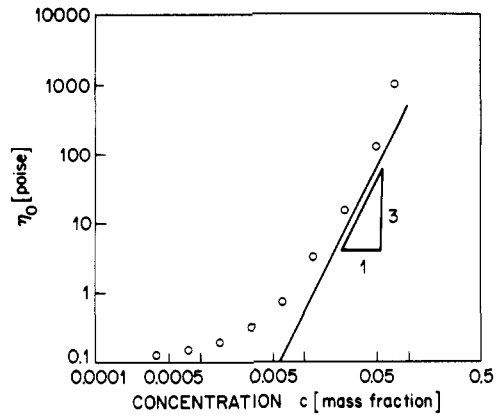

Figure 5. Zero-shear viscosity versus concentration for PBLG.

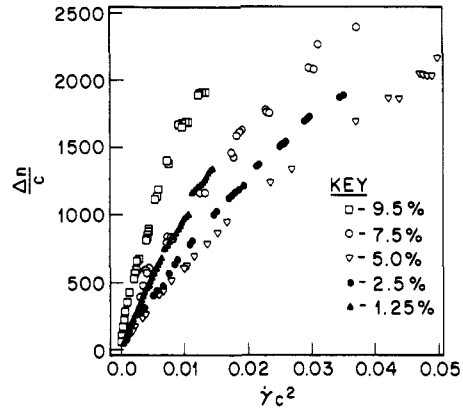

Figure 6. Birefringence versus shear rate for PBLG plotted using semidilute scaling. The concentration c is the mass fraction of polymer, and the shear rate is in s^{-1}.

The zero-shear viscosities $\eta_0 \equiv \eta(\dot{\gamma} \to 0)$ are plotted against concentration in Figure 5. At concentrations less than 2.5%, the slope of this low–log plot is less than 3; at concentrations greater than 5%, it is greater than 3. Thus the window of semi-dilute behavior—where the slope is 3—is so narrow for our materials that it is almost nonexistent; just as the concentration becomes high enough for semidilute theory to hold, an excluded-volume effect apparently begins to occur. Because our PBLG molecules are only about half as long as the collagen molecules studied by Chow et al.,[6] one would expect our semidilute window to be somewhat narrower than theirs. However, the greater polydispersity of our materials probably also plays a role. Increased polydispersity would be expected to increase the extent of overlap of the different concentration regimes. Some flexibility in the molecule might also narrow the semidilute regime. Jain and Cohen[23] have also noted that the regime of semidilute behavior for PBLG is extremely narrow or nonexistent.

Figure 6 is the birefringence plotted against shear rate, with the axes scaled with concentration in such a way that the curves would superpose in the semidilute regime. As was seen in the viscosities, at concentrations of less than 5%, the birefringence on the rescaled plot is consistent with a dependence of the relaxation time λ on c that is weaker than that of the semidilute regime, while for $c > 5\%$, the dependence is greater than that of semidilute theory.

At concentrations of 2.5% and higher, we believe that all three effects that are characteristic of the isotropic concentrated regime (as discussed in section II.C) occur

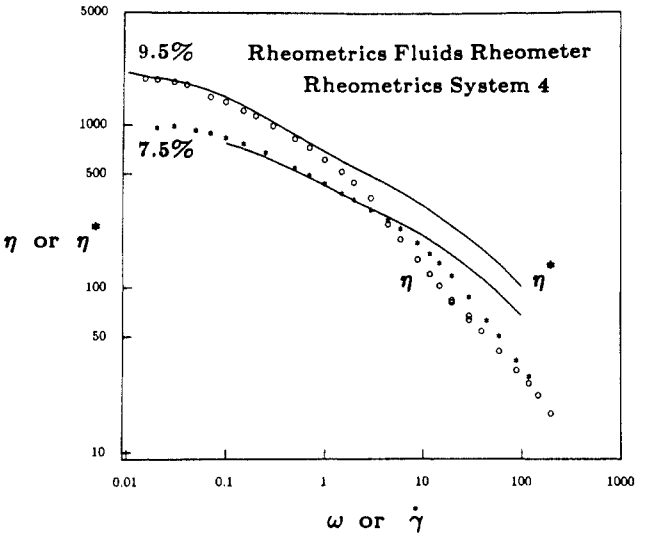

Figure 7. Steady shear (η) and dynamic (η^*) viscosity for PBLG solutions as functions of shear rate γ or frequency ω. The dynamic data were measured on the fluids rheometer, and the steady data were obtained on the system 4.

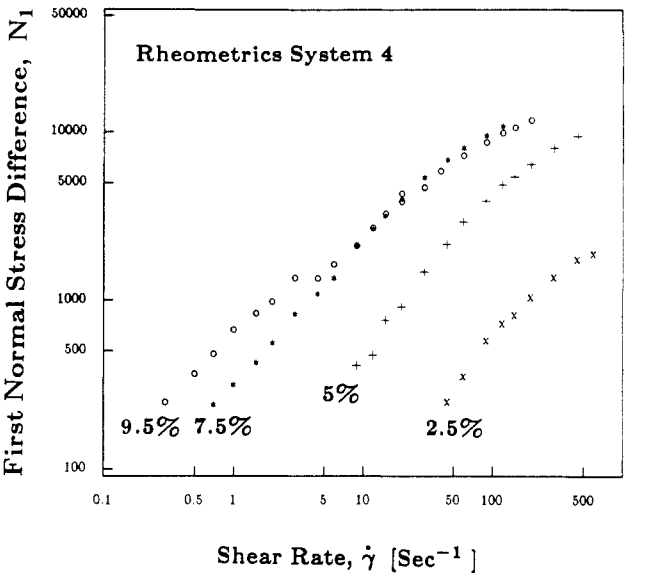

Figure 8. First normal stress difference in dyn/cm^2 as a function of shear rate for PBLG.

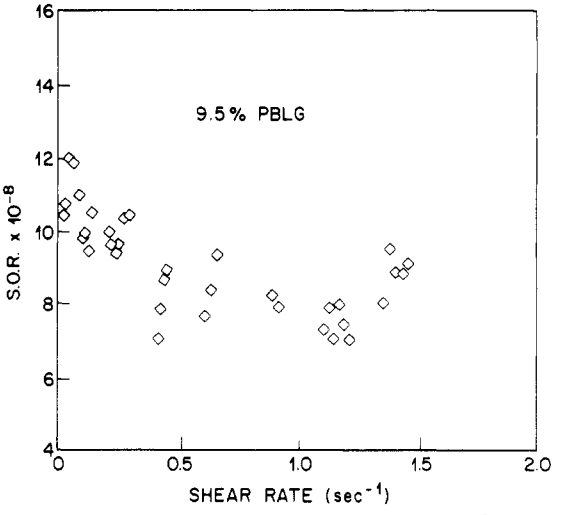

Figure 9. Stress-optical ratio n_{12}/σ_{12} in units of cm^2/dyn measured as a function of shear rate for 9.5% PBLG.

in our materials. These effects are critical slowing down, rod jamming, and nonlinear coupling between the shearing field and the excluded-volume potential. To isolate the three effects individually, we first recognize that the latter is a nonlinear effect. Thus it cannot occur in small amplitude oscillatory shearing where the flow introduces no tendency toward alignment. In Figure 7 the dynamic viscosity η^* measured in small amplitude shearing is plotted as a function of frequency ω along with the steady shear data plotted against shear rate γ for the 7.5% and 9.5% solutions. Note that at low shear rates, the steady shear viscosities agree with the dynamic viscosities. Agreement of these two viscosities is called the Cox–Merz relationship,[24] and it is often observed to hold for melts and solutions of flexible polymers.[25,26] For solutions of rods near the liquid-crystalline transition it fails at higher shear rates, however, probably because of the nonlinear coupling of the excluded-volume potential to the shearing field. Note that the steady shear viscosity for the 9.5% solution crosses that for the 7.5% solution, a phenomenon also reported by Kiss and Porter.[27] A second crossing at higher shear rates is also seen in our data in Figure 7. This double crossing of shear viscosities agrees with the prediction of the Doi theory, shown in Figure 3. In the Doi theory, values for U of 2.66 and 2.0 roughly correspond to our concentrations of 9.5% (just below the transition) and 7.5%. Furthermore, the first normal stress difference $N_1 \equiv \sigma_{11} - \sigma_{22}$ of the 9.5% solution abruptly intersects N_1 for the 7.5% solution at a shear rate near the value at which the viscosities cross; see Figure 8. The dynamic viscosities in Figure 7 do not cross; thus the crossover is a nonlinear phenomenon as predicted.

We did not observe the increase in the stress-optical ratio n_{12}/σ_{12} as a function of shear rate predicted by the Doi theory (see Figure 2) for solutions near the transition, except perhaps at the highest shear rates for which this ratio could be measured. (At high shear rates, birefringences become so large that multiple order crossings—eight or more—occur and the extinction angle becomes very hard to determine.) Figure 9 shows a gradual decrease in this ratio as a function of shear rate and perhaps a rise at the highest shear rates. The discrepancy between this result and the Doi theory is as yet unexplained, although sample polydispersity is one likely contributor.

As discussed in section II.C, only rod jamming should affect the zero-shear viscosity η_0; critical slowing down has no effect. Because of rod jamming, a log–log plot of η_0 versus concentration c should have a slope greater than 3 near the transition. This is what we observe in Figure 6. Others have also noted this phenomenon in PBLG and other rigid polymers.[16,28]

On the other hand, only critical slowing down shows up in the stress-optical coefficient; rod jamming has no effect. We therefore plot the stress-optical ratio $C_{12} \equiv n_{12}/\sigma_{12}$ extrapolated to zero-shear rate against concentration in Figure 10. The value of C_{12} is greater than 3 $\times 10^{-8}$ cm^2/dyn, more than 2 orders of magnitude larger than that typical of flexible polymers. Furthermore, it increases with concentration, in qualitative agreement with the Doi theory. The total rise in C is a factor of 3.5, in contrast with the predicted value of 5.64 alluded to earlier for the Onsager theory. The most likely explanation for this discrepancy is that polydispersity of our sample broadens the biphasic range of concentrations[29,30] and therefore cuts off the rise in C at a lower value than would be the case for monodisperse solutions of perfectly rigid rods.

As noted earlier, for perfectly rigid polymers we expect C to be directly proportional to molecular weight. For

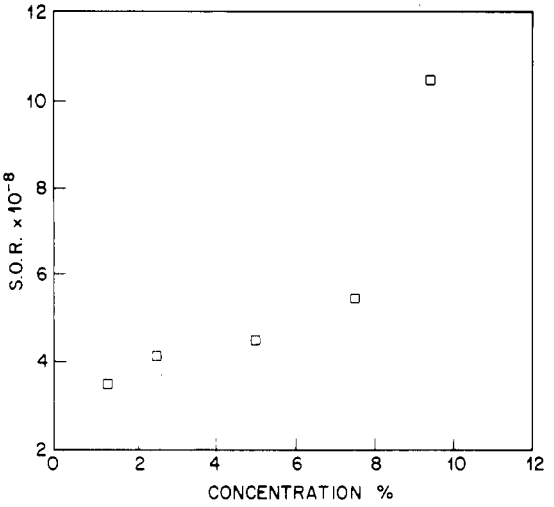

Figure 10. Stress-optical ratio n_{12}/σ_{12} in units of cm^2/dyn at low shear rate measured as a function of concentration of PBLG.

an isotropic solution of 25% PBLG of molecular weight 23 000, we found a value C_{12} of 0.58×10^{-8}, about 8 times lower than the value for PBLG of molecular weight 230 000 at concentrations well away from the transition. Thus a 10-fold increase in molecular weight produces an 8-fold increase in C. This behavior is consistent with that reported by Tsvetkov and co-workers,[5] whose calculations show that this degree of departure from a linear dependence of C_{12} on molecular weight is about whan one would expect for a molecule with the persistence length of roughly 90 nm. which is the value reported by Parthasarathy et al. for PBLG in *m*-cresol.[15] The persistence length of PBLG can vary by a factor of 2 or more depending on the solvent.[15]

The dependence of C on molecular weight implies that for polydisperse samples—such as ours and those of most workers—there will be violations of the stress-optical rule in the nonlinear viscoelastic regime. This is so because changes in shear rate change the relative degree to which each portion of the molecular weight distribution is oriented in flow; this ought to produce a shift in C. At low rates of shear, only long rods orient significantly; at higher shear rates more of the short rods orient. Thus by itself, polydispersity should tend to cause C to decrease with increased shear rate. Such a tendency can indeed be discerned in Figure 9. A more dramatic effect is expected, however, when a strong shearing flow suddenly ceases. During the strong flow, both long and short rods orient and C reflects an average of all rods. Since the short rods reorient quickly relative to the long rods, one would expect the short rods to stop contributing to C shortly after shearing ceases, while long rods remain oriented and contribute to C for some time longer. Thus an increase in the stress-optical coefficient afte cessation of steady shearing is to be expected. The higher the steady shear rate, the more oriented the short rods are during shearing, and the greater the increase should be after cessation of shear.

This behavior is evident in the data present in Figure 11 for start-up and cessation of steady shearing of 9.5% PBLG. After cessation of a strong shearing flow, an increase of C by a factor of 2 is recorded. Note that immediately after the start of steady shearing there is a rise and overshoot in C before a steady state is reached. This behavior can also be rationalized in terms of the differing rates at which long and short rods reach a steady-state orientation after start-up of steady shearing. In all, during start-up and cessation of steady shearing in Figure 11a, C changes by a factor of 3. This shows that molecular weight components differing by a factor of 3 or more contribute significantly to the molecular weight distribution of our samples, which is consistent with the level of polydispersity, $M_w/M_n \approx 1.8$, of our material. The changes in C after cessation of steady shearing of PBLG solutions are demonstrably *not* instrumental artifacts. Figure 12 shows that for a solution of flexible polystyrene molecules, no such variations in C occur after start-up and cessation of shearing. The oscillations present in the data of Figure 11 after cessation of shearing arise from instrumental measurement errors that occur when the birefringence passes through fringe orders. These errors can be avoided in measurements during small amplitude oscillatory shearing, where the birefringence is kept low by the smallness of the strain amplitude. Variations in C that can be attributed to polydispersity are seen in

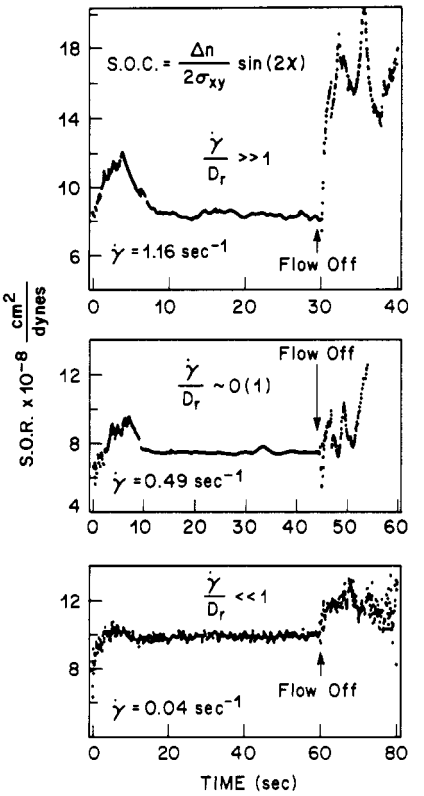

Figure 11. Dependence of the stress-optical ratio n_{12}/σ_{12} on time for 9.5% PBLG after start-up and cessation of steady shearing at three different rates of shear.

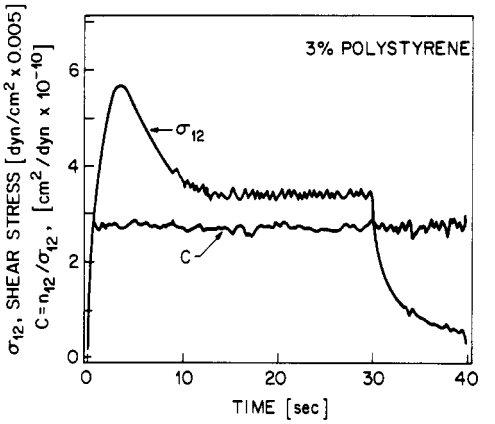

Figure 12. Dependence of the shear stress and the stress-optical coefficient on time for a 3% solution of polystyrene in tricresol phosphate after start-up and cessation of steady shearing at the rate $\dot{\gamma} = 0.91\ s^{-1}$. The molecular weight of the polystyrene is 8 million.

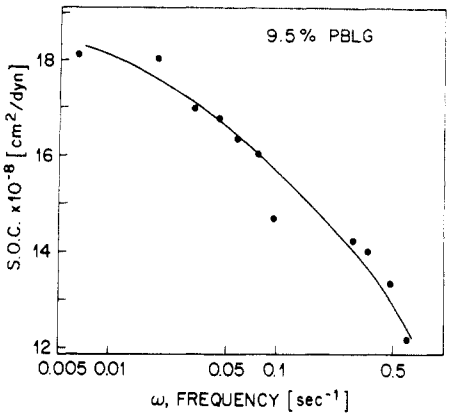

Figure 13. Stress-optical ratio as a function of frequency in small-amplitude oscillatory shearing for 9.5% PBLG.

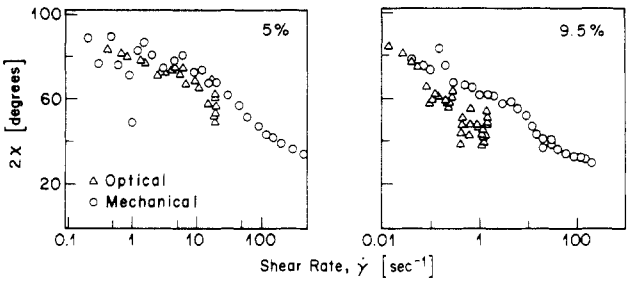

Figure 14. Twice the optical and mechanical extinction angles as functions of shear rate for 5% and 9.5% PBLG.

the frequency regime as well as in the time regime. Figure 13 shows C as a function of frequency in small-amplitude oscillatory shearing for 9.5% PBLG. At low frequency, where only the longest rods are sluggish enough to respond, C is around 18×10^{-8}, consistent with the value obtained some time after cessation of steady shear in Figure 11. As frequency increases, the shorter rods begin to respond as well, bringing the average value of C down as low as 12×10^{-8}.

As discussed in section II.C, the Doi theory for monodisperse rods predicts that the stress tensor should be coaxial with the birefringence tensor at any concentration and at any shear rate. This prediction holds at modest levels of orientation attained in the 5% solution as can be seen in Figure 14, but for the higher birefringences achieved in the 9.5% solution, the mechanical and optical χ values appear to be significantly different. This again could be a polydispersity effect. Since long rods have a higher stress-optical coefficient than do short rods, the long rods should contribute more strongly to the optical measurements than to the mechanical measurements. Since the long rods are expected to be more oriented than the short rods, their influence should reduce the effective χ values more in the birefringence measurements than in the mechanical measurements, which is consistent with our observations.

A quantitative prediction of the noncoaxiality of the mechanical and optical tensors, of the shear rate, time dependence, and frequency dependence of C, and of the other data presented here will require use of a version of the Doi theory generalized to allow for polydispersity. Such a theory has been proposed by Marrucci and Grizutti[31] and has been found successful in predicting rheological properties of rodlike polymers in the semidilute regime.[6] Efforts are under way to apply this theory to our measurements in the concentrated isotropic regime.

V. Concluding Remarks

The new phenomena reported here for a rodlike polymer in the concentrated isotropic regime include the dependence of the stress–optical ratio C on molecular weight, concentration, shear rate, and even time after start-up and cessation of steady shearing. We have also found that the stress and birefringence tensors are not coaxial at concentrations close to the transition. Thus for these fluids, the concept of a linear stress–optical law fails in every possible sense.

In addition, we have found a double crossover of viscosity–shear rate curves measured for different concentrations close to the liquid-crystalline boundary, indicative of nonlinear cooperatively between the shear field and the excluded-volume potential. This effect is qualitatively consistent with the Doi theory, as is the concentration dependence of C. Polydispesity effects are seen in the dependence of C on shear rate and on time and apparently also in the lack of coaxiality of the stress and birefringence tensors. These effects, especially the time dependence of C, may yield provide a valuable means of estimating molecular weight distributions for stiff polymers.

Acknowledgment. We gratefully acknowledge and thank Robert Boie of Bell Labs for his advice in the design of the stress transducer and C. S. Lee of the University of Utah for intrinsic viscosity measurements.

References and Notes

(1) Doi, M.; Edwards, S. F. *The Theory of Polymer Dynamics*; Oxford Press: London, 1986.
(2) Bird, R. B.; Curtiss, C. F.; Armstrong, R. C.; Hassager, O. *Dynamics of Polymeric Liquids*; 2nd ed.; Wiley: New York, 1987; Vol. 2.
(3) Janeschitz-Kriegl, H. *Polymer Melt Rheology and Flow and Birefringence*; Springer-Verlag: New York, 1983.
(4) Muller, R.; Froelich, D. *Polymer* **1985**, *26*, 1477.
(5) Tsvetkov, V. N.; Andreeva, L. N. *Adv. Polym. Sci.* **1981**, *39*, 95.
(6) Chow, A. W.; Fuller, G. G. *Macromolecules* **1985**, *18*, 786. Chow, A. W.; Fuller, G. G.; Wallace, D. G.; Madri, J. A. *Macromolecules* **1985**, *18*, 793, 805.
(7) de Gennes, P.-G. *Mol. Cryst. Liq. Cryst.* **1971**, *12*, 193.
(8) Nakamura, H.; Okano, K. *Phys. Rev. Lett.* **1983**, *50*, 186.
(9) Onsager, L. *Ann. N.Y. Acad. Sci.* **1949**, *51*, 627.
(10) Lasher, G. *J. Chem. Phys.* **1970**, *53*, 4141.
(11) Odijk, T. *Macromolecules* **1986**, *19*, 2313.
(12) Doi, M. *J. Phys. (Les Ulis, Fr.)* **1975**, *36*, 607.
(13) Edwards, S. F.; Evans, K. E. *J. Chem. Soc., Faraday Trans. 2* **1982**, *78*, 113.
(14) Hermans, J., Jr. *J. Colloid Sci.* **1962**, *17*, 638.
(15) Parthasarathy, R.; Houpt, D. J.; Dupre, D. B. *Liq. Cryst.* **1988**, *3*, 1073.
(16) Enomoto, H.; Einaga, Y.; Teramoto, A. *Macromolecules* **1984**, *17*, 1573.
(17) Larson, R. G.; Mead, D. W. *J. Rheol.*, in preparation.
(18) Larson, R. G.; Mead, D. W. *J. Rheol.* **1989**, in press.
(19) Experiments in the system 4 were done without temperature control because the temperature control on this instrument was a convection oven, the use of which we felt could pose a risk of solvent evaporation. The temperature of the material in the system 4 was always brought to within 2 °C of 29 °C, however, by circulating transducer fluid. In fact, 29 °C was chosen as the operating temperature for the other instruments to match the temperature in the system 4, and viscoelastic measurements in the system 4 were consistent with those obtained in the other instruments; see Figure 7 for example.
(20) Osaki, K.; Kimura, S.; Kurata, M. *J. Polym. Sci., Polym. Phys. Ed.* **1981**, *29*, 517.
(21) Frattini, P. L.; Fuller, G. G. *J. Colloid Interface Sci.* **1984**, *100*, 506.
(22) Larson, R. G.; Khan, S. A.; Raju, V. R. *J. Rheol.* **1988**, *32*, 145.
(23) Jain, S.; Cohen, C. *Macromolecules* **1981**, *14*, 759.
(24) Cox, W. P.; Merz, E. H. *J. Polym. Sci.* **1958**, *28*, 619.
(25) Utracki, L. A.; Gendron, R. *J. Rheol.* **1984**, *28*, 601.

(26) Larson, R. G. *Rheol. Acta* **1985**, *24*, 327.
(27) Kiss, G.; Porter, R. S. *J. Polym. Sci., Polym. Symp.* **1978**, *65*, 193.
(28) Venkatraman, S.; Berry, G. C.; Einaga, Y. *J. Polym. Sci., Polym. Phys. Ed.* **1985**, *23*, 1275.
(29) Frost, R. S.; Flory, P. J. *Macromolecules* **1978**, *11*, 1134.
(30) Lekkerkerker, H. N. W.; Coulon, P.; van der Haegen, R.; Deblieck, R.; *J. Chem. Phys.* **1984**, *80*, 3427.
(31) Marrucci, G.; Grizzuti, N. *J. Non.-Newtonian Fluid Mech.* **1984**, *14*, 103.

Fractal Nature of One-Step Highly Branched Rigid Rodlike Macromolecules and Their Gelled-Network Progenies

S. M. Aharoni*

Polymer Science Laboratory, Allied-Signal Research and Technology, Allied-Signal Inc., P.O. Box 1087R, Morristown, New Jersey 07962

N. S. Murthy and K. Zero

Analytical Sciences Laboratory, Allied-Signal Research and Technology, Allied-Signal Inc., Morristown, New Jersey 07962

S. F. Edwards

Cavendish Laboratory, Cambridge University, Madingley Road, Cambridge CB3 0HE, U.K.
Received September 14, 1989; Revised Manuscript Received November 20, 1989

ABSTRACT: Several highly branched polymeric systems were prepared by a one-step polymerization. They are characterized by stiff trifunctional branchpoints connected by rigid rodlike segments. A few systems with flexible segments were prepared for comparison. The systems were studied in their pregel and postgel states. Small-angle X-ray scattering intensity measurements from bone-dry and concentrated solutions are consistent with the expectations of the polymeric fractal model. Static light scattering combined with photon correlation spectroscopy revealed the polymeric species in the pregel state to be highly branched. End-group titration and segment-tip decoration by iodine clearly indicate the highly branched nature of the pregel as well as postgel systems. The kinetics of particle growth prior to the gel point and solution property characteristics both agree with the fractal model. Scanning electron microscopy of the dried pregel material yielded typical fractal morphology. Porosimetry studies of one dry postgel network supports the fractal concept. When compatible macromolecular fillers were added to the reaction mixture of the one-step systems prior to the gel point, the modulus of the resulting "infinite" network gels was consistently lower than the modulus of the corresponding neat gel. When the rigid networks were prepared in two steps from preexisting high-M chains, their modulus increased upon the addition of the same filler macromolcules. The weakening effect of filler macromolecules was even more dramatic in the case of one-step flexible polymer gels. When short, monodisperse oligomers were added to the one-step rigid networks instead of their long filler analogues, no effect on the modulus was observed. We propose two growth morphologies to explain our observations. In the one-step polymerization, random nucleations form polymer fractals. They cluster together and when a sufficient number of them grow enough, a contiguous network is formed that, when reaching from one end of the sample to the other, is best described as an "infinite" cluster of polymeric fractals. At this point gelation occurs. Further reaction more or less fills the sample volume with additional fractals, which may or may not be covalently attached to the "infinite" network. The filler macromolecules are pushed ahead of the fractal growth fronts until trapped in between. Thus they reduce the concentration of strong bonds between fractals and clusters causing a reduction of the modulus of the ensemble as a whole. The oligomers are shorter than the network's segments, so they can be accommodated within the growing fractal and not affect the modulus of the gelled network. In the case of two-step network formation, the solution is randomly filled with high-M macromolecules and when these cross-link the system rapidly gels with only minor variations in local cross-link concentration. Long filler macromolecules appear not to measurably interfere with the formation of interchain bonds. Hence, the modulus of the network does not decrease.

Introduction

Until recently, most theoretical treatments studied covalent polymeric networks that consist of flexible Gaussian segments cross-linked by residues of fully reacted functionalities.[1,2] The mathematics of the standard approach was in the spirit of the mean-field theory. The material was considered essentially homogeneous with cross-links uniformly arranged through it (physical assumption) and the closed loops and other imperfections treated as perturbations (a mathematical assumption). Moreover, polymer chemistry provided networks of short monomers and flexible long segments. All these conditions can be changed through the introduction of rigid segments interconnected at stiff or flexible branchpoints, and the corresponding mathematics has to respond. Thus, the basic papers[3-8] have to be modified when rigid rodlike polymers comprise the network rather than flexible ones. In their unbranched and un-cross-linked form, these rodlike polymers are liquid crystalline in nature.

There are three fundamentally different methods of preparing gelled, covalently linked polymeric networks. One is to start with a solution of the appropriate monomers, whose average functionality is higher than 2.0, and conduct the polymerization in a single step. This procedure will be called here a one-step method. The growing polymeric entities are highly branched and, as will

0024-9297/90/2223-2533$02.50/0